JOURNAL OF MATERIALS SCIENCE 23 (1988) 4503–4512

Thermal evolution and densification of R_2O–SiO_2 gels

M. A. VILLEGAS, J. M. FERNÁNDEZ NAVARRO
Instituto de Cerámica y Vidrio, CSIC Arganda del Rey, Madrid, Spain

R_2O–SiO_2 materials were prepared with 5 mol% of alkaline oxide by the sol–gel method. The gel–glass transition was achieved by treatment in air or in a controlled atmosphere. The samples present a silica network structure to which the alkaline ions are incorporated in a different way as compared to that of conventional glass. Material densification sets in around 350° C. In the temperature range between 500 and 600° C silica devitrification are produced together with condensation–polymerization of many silanol groups which form part of the material. Densification treatments in a helium atmosphere eliminate these residual groups.

1. Introduction

In recent years alkaline silicate glasses as obtained through the sol–gel method have been widely studied. In particular materials derived from Na_2O–SiO_2 gels have been prepared from different precursors under varying experimental conditions, so that a considerable variety of synthesis methods and the respective research is available.

It is a well known fact that it is the distinctive feature of sol–gel alkaline silicate materials to show a marked trend towards alkaline salt crystallization and devitrification [1–8]. This problem is due to carbonation during gel drying and the elevated volume of water generally required for preparation.

With the aim of avoiding crystallizations and preserving at the same time the monolithic shape of the pieces, several authors [8–10] have used drying control chemical additives (DCCAs) during sol preparation. The most commonly employed DCCAs are formamide and triethylorthoformiate, both capable of being adsorbed to the gel surface, thus accelerating the drying process. The use of DCCAs, however, is no guarantee that the resulting product is a monolithic, crystallization-free piece. In addition, DCCA elimination possesses certain problems [8–10].

Another characteristic feature of gel-derived alkaline silicate glasses is that they are much less resistant to corrosion or hydrolitic attack than the respective conventional glasses, which is indicative of the fact that alkaline ion incorporation into the silica gel structure does not occur by strong bonds. This same fact also accounts for the great mobility of these ions in the structure [12–14]. Aided by the high level of adsorbed water, the ions give rise to a porous structure impregnated with water molecules H-bonded to the terminal silanol groups. On the other hand, the presence of water originates a much more straightforward phase separation than those that occur in conventional glasses of the same composition [15–17]. The features and properties of these materials make them especially suited as ion conductors at low temperatures [12–13], and as vitroceramics [18].

In this research alkaline silicate glasses are prepared by the sol–gel process with one or two alkaline oxides in order to study their densification behaviour as well as their thermal and structural evolution.

2. Experimental

2.1. Sample preparation

Gels of the system R_2O–SiO_2 (R = K, Na, Li, K + Na, K + Li and Na + Li) were prepared with 5 mol% of alkaline oxide(s) (Table I). The experimental method for sol preparation as well as gelling and heat treatment have been described in previous works [11–14]. In addition to heat treatments in air to densify the material, further treatments were carried out in helium, nitrogen and Cl_2–He (50 vol%) atmospheres with the aim of studying the potential release of structural and molecular water [19–21]. These treatments were preformed at an approximate total flow rate of 8 ml sec^{-1}.

2.2. Densification study and thermal evolution of the samples

Gel densification was studied by dilatometry and specific surface area and density measurements. Thermal evolution and gel–glass transition were followed by means of IR absorption spectroscopy and near IR (NIR) diffuse reflectance spectroscopy. Gel texture was observed by scanning electronic microscopy (SEM).

The IR absorption spectra were recorded on a Perkin Elmer spectrophotometer, model 580 B, using powdered

TABLE I Sample compositions

Sample	Mol%			
	K_2O	Na_2O	Li_2O	SiO_2
1.1	5	–	–	95
1.2	–	5	–	95
1.3	–	–	5	95
1.4	2.5	2.5	–	95
1.5	2.5	–	2.5	95
1.6	–	2.5	2.5	95

0022–2461/88 $03.00 + .12

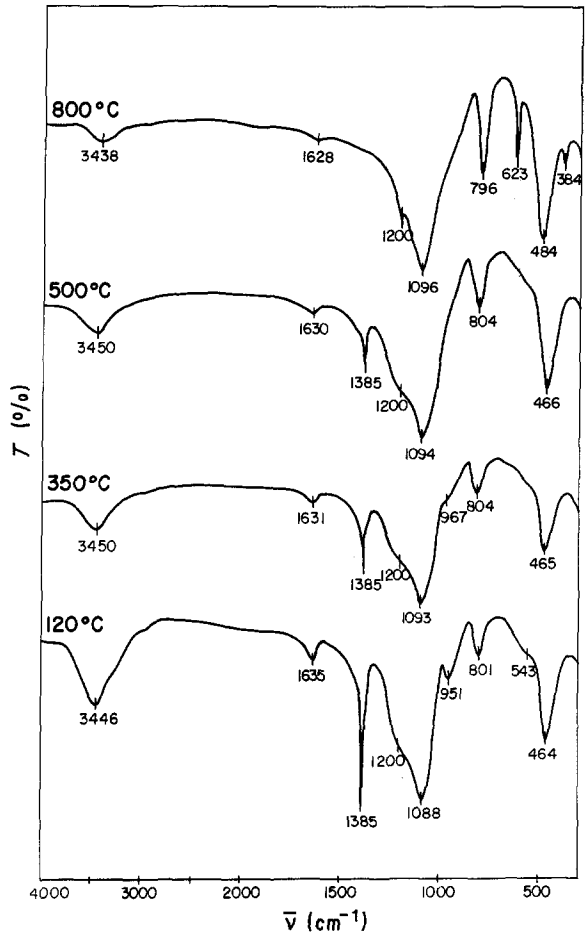

Figure 1 IR spectra of gel 1.2 at different temperatures.

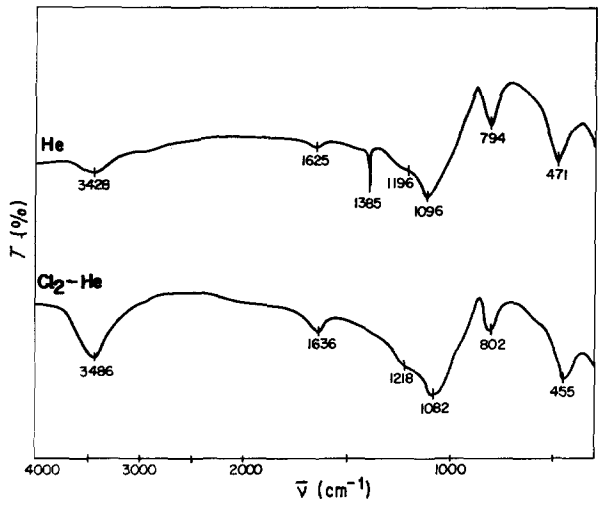

Figure 2 IR spectra of gel 1.2 (600° C) treated in helium and Cl_2–He.

samples diluted in anhydrous KBr pellets. The NIR diffuse reflectance spectra were obtained on a Perkin Elmer Lambda 9 apparatus, also from powdered samples. For SEM observations two groups of recently fractured samples were used: on the one hand, samples heat treated at 120° C without attack, and on the other, samples heat treated at 500° C which had been subjected to 10% HF attack for 30 sec.

The expansion curves were recorded on an Adamel Lhomargy DI-24 apparatus, with heating rates of $1°C\,min^{-1}$ and Al_2O_3 as a carrier substance. The planoparallel samples used were prepared from gel pieces polished with silicon carbide paper. The specific surface area was determined with the BET method on a Micromeritics set, model AccurSorb 2100 E. Densities were determined directly measuring the volume of the powdered samples on a pycnometer and using toluene as a reference liquid.

3. Discussion of results

3.1. IR absorption spectra

Fig. 1 shows the IR absorption spectra in the range of 300–4000 cm^{-1} for sample 1.2 ($5Na_2O$–$95SiO_2$). The most relevant vibration band assignments are compiled in Table II. The bands attributed to the silica network (1200, 1090, 800 and 465 cm^{-1}) evolved with temperature, becoming more peaked and better defined. The band corresponding to the O–Si–O deformation vibration (465 cm^{-1}) does not appear in the spectrum of the sample treated at 800° C. It is moreover replaced by three bands (623, 484 and 384 cm^{-1}) due to Si–O vibration of the α-cristobalite network which is formed around 800° C [11]. On the other hand, the stretching vibration of the Si–OH bond (955 cm^{-1}) is a shoulder in the sample treated at 350° C and disappears with increasing temperature. This fact, together with the diminishment of the C–H deformation band of the methyl groups (1385 cm^{-1}) is indicative of the release of residual organic groups and the onset of densification in the temperature range of 350 to 500° C. The intensity of the band assigned to the H–O–H deformation vibration of water (1630 cm^{-1}) diminishes with increasing heat-treatment temperature. The fact that this band does not completely vanish is due to the rehydration of the samples during handling.

The spectra of the remaining samples present bands at the same wavelengths, hence showing a thermal evolution which is identical to that described for sample 1.2. This is explained by the fact that the alkaline ions practically are not incorporated into the silica network [11–14], since the non-bridging oxygen ions are blocked forming silanol groups. The alkaline cations are probably positioned at the interstitial gaps of the silica particles. This would explain why, whatever ion or ions are present, the vibrations detected by IR spectroscopy always refer to a silica network with a greater or lesser degree of polymerization. The IR spectra of the 1.2 samples treated at 600° C in helium and Cl_2–He atmospheres (Fig. 2) present the typical absorption bands of a silica network (1200, 1090, 800 and 465 cm^{-1}). The spectrum of the gel treated in

TABLE II IR frequencies (cm^{-1}) and vibration assignments for sample 1.2

$\bar{\nu}$ (cm^{-1})	Assignment	References
1630	H–O–H deformation	[22]
1385	C–H deformation	[23]
1200	Asymmetric Si–O stretching (longitudinal optical mode)	[24]
1090	Asymmetric Si–O stretching (transverse optical mode)	[5, 22, 24–26]
955	Stretching Si–OH	[5, 24, 26]
800	$[SiO_4]$ tetrahedra rings	[5, 22, 24, 25]
623	Si–O vibration in cristobalite	[27]
484		
384		
465	O–Si–O deformation	[5, 22, 25]

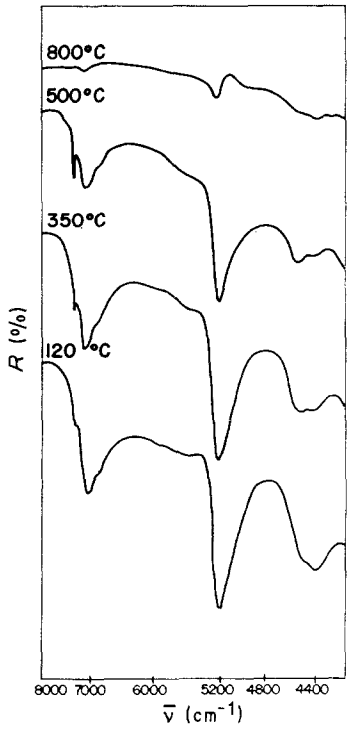

Figure 3 NIR spectra of gel 1.2 at different temperatures.

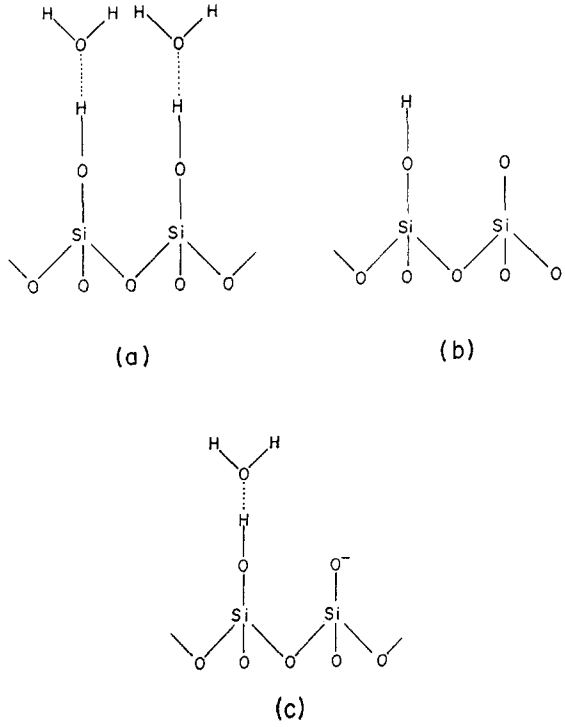

Figure 4 Molecular structures of a pure silica gel according to Wood *et al.* [32].

helium shows an additional small peak at 1385 cm^{-1} due to residual organic groups. The absence of oxygen during heat treatment can be accounted by a slower combustion process of the residual groups. The bands due to water (3470 and 1630 cm^{-1}), are larger in the spectrum of the sample treated in Cl_2–He than in the sample treated in helium. X-ray diffraction data proved the presence of NaCl in the sample treated in Cl_2–He. Chlorine is able to react with the Na^+ ions which have not been incorporated into the silica network. The presence of the highly hygroscopic NaCl may have retained a greater amount of water during later handling of the sample. The IR absorption spectrum of gel 1.2 treated at 600° C in a nitrogen atmosphere, showed practically the same bands as in the spectrum of the same gel densified at 500° C in air, although the water bands are slightly fainter.

3.2. NIR diffuse reflectance spectra

The absorption spectra in the near IR have been obtained previously [14] for all samples. These spectra were recorded for the temperature range from 120 to 300° C using thin slab samples. The appearance of cracks in the samples detected at 300° C as a consequence of drying and the onset of densification, makes it impossible to obtain spectra for samples treated at higher temperatures by this method. In order to overcome this constraint, in the advanced stages of the densification process (above 350° C), the evolution of the silanol groups and residual molecular water release were studied through diffuse reflectance spectra in the range of the near IR utilizing powdered samples.

Fig. 3 shows the NIR spectra (4200–8000 cm^{-1}) for sample 1.2. Band assignment (Table III) was done according to the criteria used in previous studies. At low temperatures, many silanol groups bonded to water molecules exist on the silica particles surface. On increasing the temperature the more externally positioned water molecules are eliminated and others are transferred from the most hydrated silanols to free positions on isolated silanols. Subsequently a further increase in temperature triggers a second loss of water molecules directly bonded to the silanols, as well as the initiation of densification with structural OH^- loss. This situation is depicted by band evolution in the spectra represented in Fig. 3. The bands due to the O–H of neighbouring silanol groups H-bonded to water molecules (7117, 4545 and 4425 cm^{-1}) as well as the combination band of the O–H of water in this structure (Fig. 4a) diminish progressively as a function of rising temperature and practically disappear at 800° C. The presence of a band at 5263 cm^{-1} in the spectrum of the sample treated at 800° C can be attributed to the combination band of the O–H of adsorbed water at a later stage during sample handling. This band shows a vibration mode similar to that of water molecules in the structure of Fig. 4a.

As regards the first O–H overtone of the free isolated silanols (7300 cm^{-1}) (Fig. 4b), the band increases up

TABLE III NIR frequencies (cm^{-1}) and assignments for sample 1.2

$\bar{\nu}$ (cm^{-1})	Assignment	References
7300	First overtone of the O–H stretching vibration of the free isolated silanol	[28–32]
7117	First overtone of the O–H vibration of the neighbouring silanols H-bonded to water	[33]
5260	Stretching-bending combination of the water O–H H-bonded to neighbouring silanols	[29–32]
4545 4425	O–H stretching-bending combination of free silanols or H-bonded neighbouring silanols	[28–32]

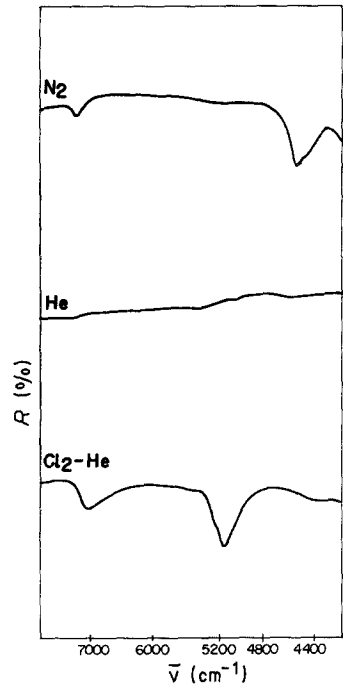

Figure 5 NIR spectra of gel 1.2 (600° C) treated in nitrogen, helium and Cl_2–He.

to 500° C as a consequence of rehydration through the water molecules from the clusters in Fig. 4a. Later on, at 800° C, this band disappears due to the final loss of water and material densification. In the case of the $5Na_20.95SiO_2$ sample (1.2) treated at 600° C in Cl_2–He, the NIR diffuse reflectance spectrum (Fig. 5) only shows two bands at 7018 and 5168 cm^{-1}. These bands are assigned [32] to the first overtone and the stretching–bending combination vibration, respectively, of the water molecules H-bonded to isolated silanols. The same gel, when heat treated at the same temperature but in a helium atmosphere did not show any reflexion vibration in that zone of the spectrum (Fig. 5). This result confirms the data obtained from IR absorption spectroscopy and supports X-ray diffraction results which evidenced the amorphous nature of this gel. In fact, the sample treated in helium is free of molecular water and structural residual OH^- groups (silanol groups), whereas the sample treated in Cl_2–He, due to the presence of NaCl formed during heat treatment, is able to retain some adsorbed water molecules and isolated silanols. For the same gel ($5Na_20.95SiO_2$) treated at 600° C in nitrogen a spectrum was recorded which only presented one low intensity band at 4545 cm^{-1} (Fig. 5). This band may be due to the existence of some residual silanols. Hence heat treatment in nitrogen does not completely eliminate the residual silanol groups. At 600° C some silanols may even remain in the material structure. Heat treatment in the presence of helium, however, does achieve complete elimination of the silanol groups at 600° C. This may be due to the low molecular weight of helium and to the high water diffusion in that gas. The spectra corresponding to the rest of the samples treated in helium and nitrogen atmospheres did not essentially differ from the situations described for gel 1.2.

3.3. Gel microstructure

Fig. 6 shows the texture of gel 1.2 treated at 120° C. The fracture surface without attack, which appears smooth and homogeneous (Fig. 6a), is slightly granulated (Fig. 6b). The other samples present a similar texture at low temperatures.

When the gels are treated at 500° C there appear α-cristobalite nuclei. The micrographs in Fig. 7 show the microstructure of HF-attacked gels. Except for the Li_2O sample (1.3), which practically presents no inhomogeneities nor crystalline nuclei, all samples show crystalline nuclei to a greater or lesser degree. As was demonstrated elsewhere [11], by means of X-ray diffraction at 500° C, incipient α-cristobalite nucleation is detectable in all samples, which increases as a function of the heat-treatment temperature. In sample 1.3 a lesser amount of α-cristobalite and the appearance of α-quartz was detected above 750° C. These results explain that the IR spectra contain bands due to the α-cristobalite network above 500° C.

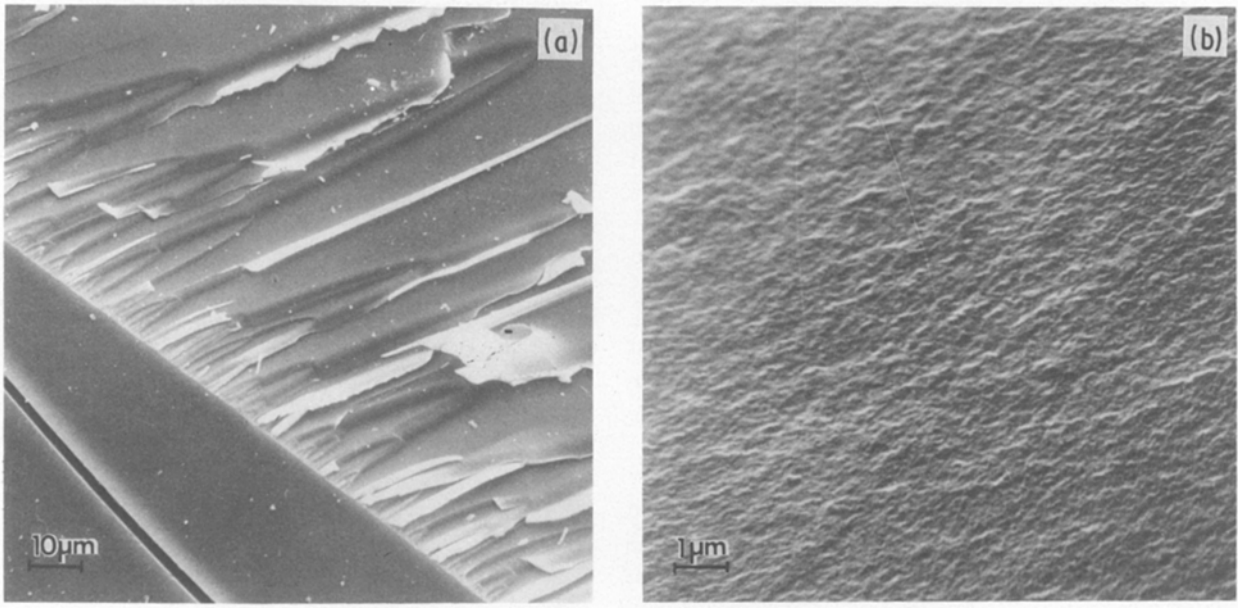

Figure 6 Micrographs of gel 1.2 heat-treated at low temperatures.

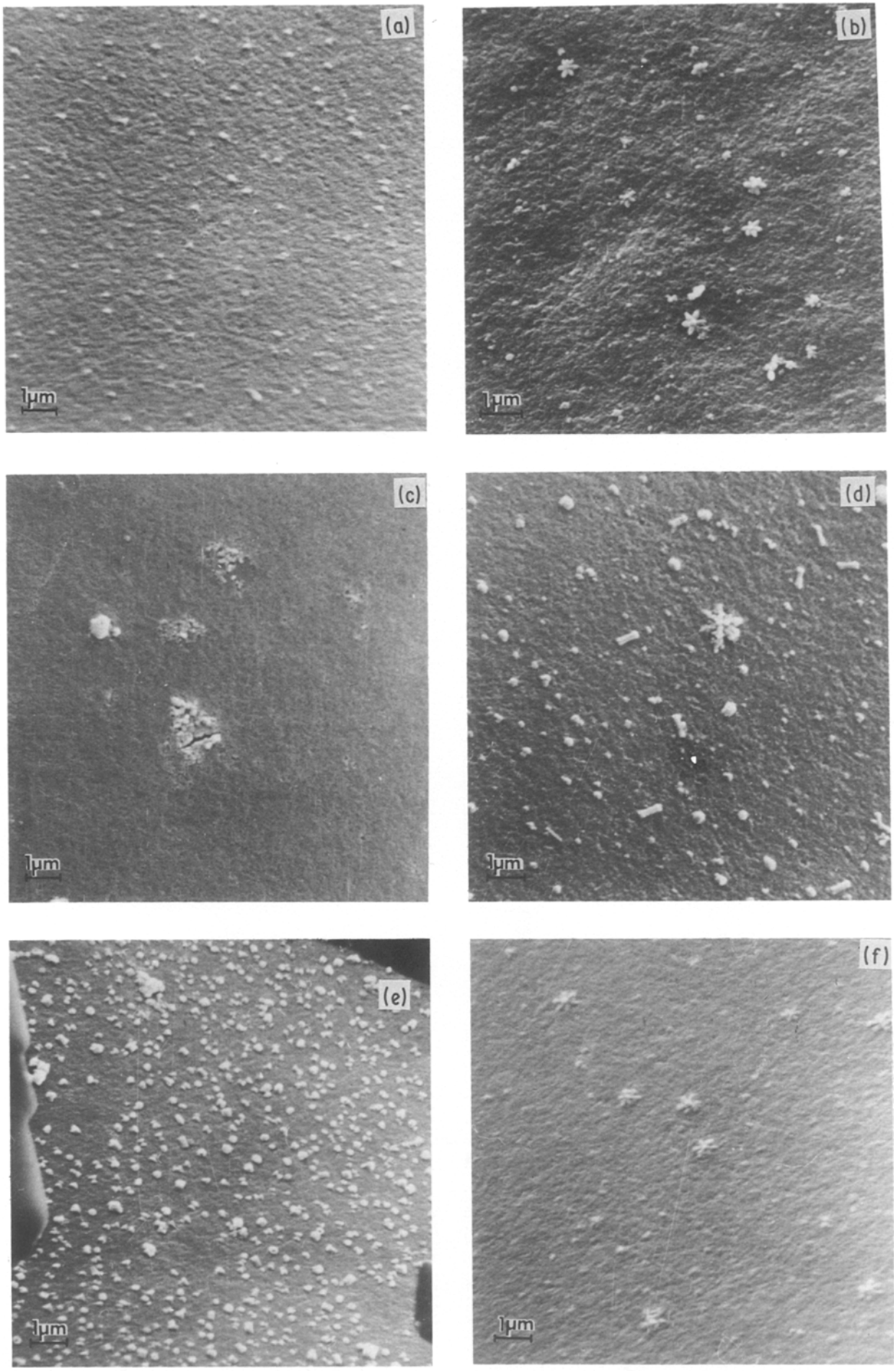

Figure 7 Micrographs of gels treated at 500° C.

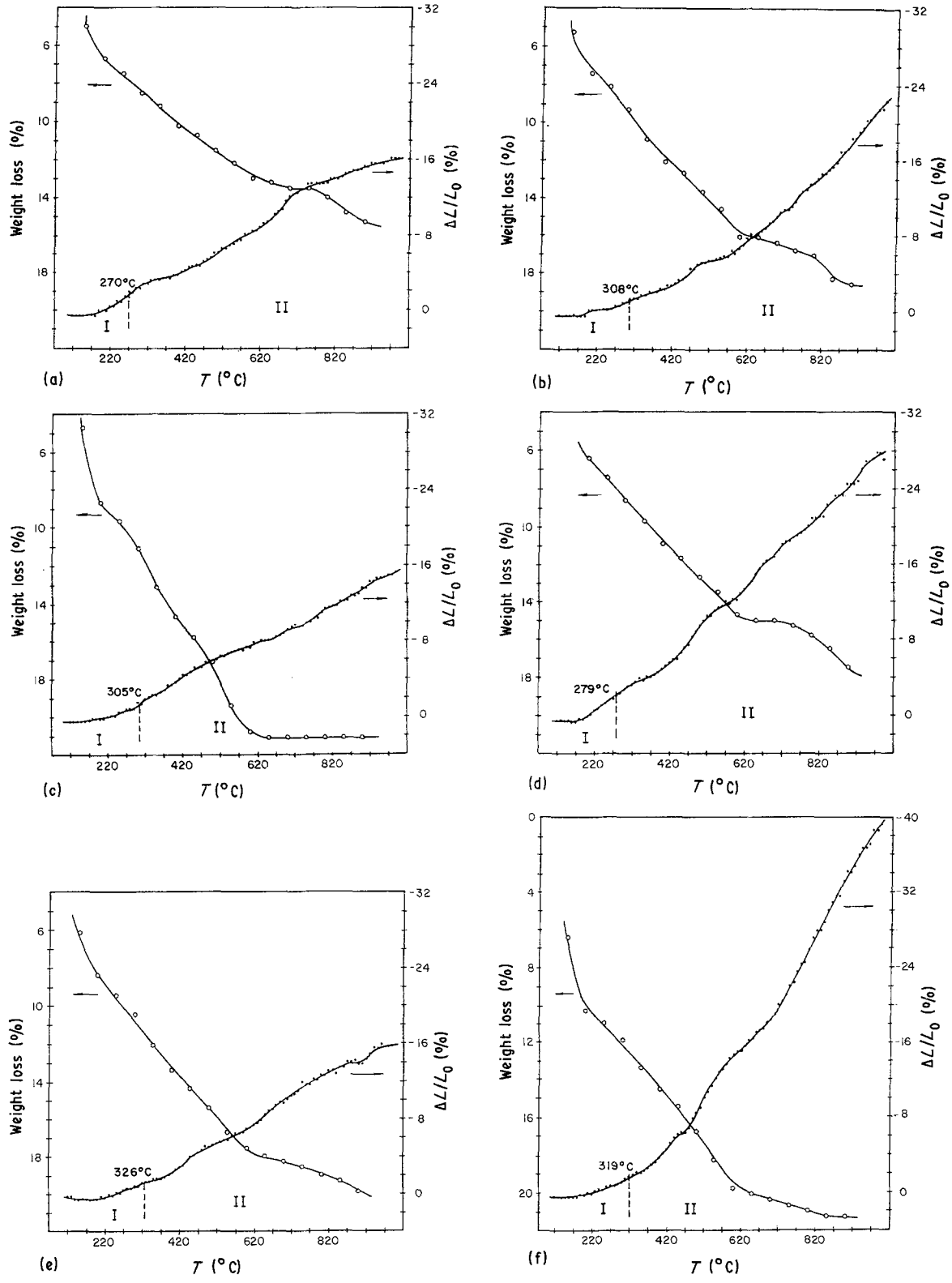

Figure 8 Linear contractions and weight losses of gels as a function of temperature per samples (a) 1.1, (b) 1.2, (c) 1.3, (d) 1.4, (e) 1.5, (f) 1.6.

3.4. Gel densification

Fig. 8 shows the linear contraction curves ($\Delta L/L_0$) plotted against temperature together with the weight loss percentages calculated from the TGA curves [11]. It must be noted that both curves were recorded at different heating rates: the dilatograms were obtained at $1°C\,min^{-1}$, whereas the TGA curves correspond to a heating rate of $10°C\,min^{-1}$. Consequently, the effects observed in the weight loss curves are retarded as a function of the different heating rate.

Gels 1.2, 1.4 and 1.6, all with Na_2O, are the ones that show a greater global linear contraction, whereas the samples containing lithium and/or potassium, contract much less as a function of temperature. This could be attributed to the action of medium size of the Na^+ ions, which account for greater amounts of water retained at higher temperatures, once they start incorporating into the network and liberate water molecules [14]. Thus the amount of water to be eliminated during the densification process is relatively greater and hence contraction is also greater.

Fig. 8 demonstrates a habit common to the six

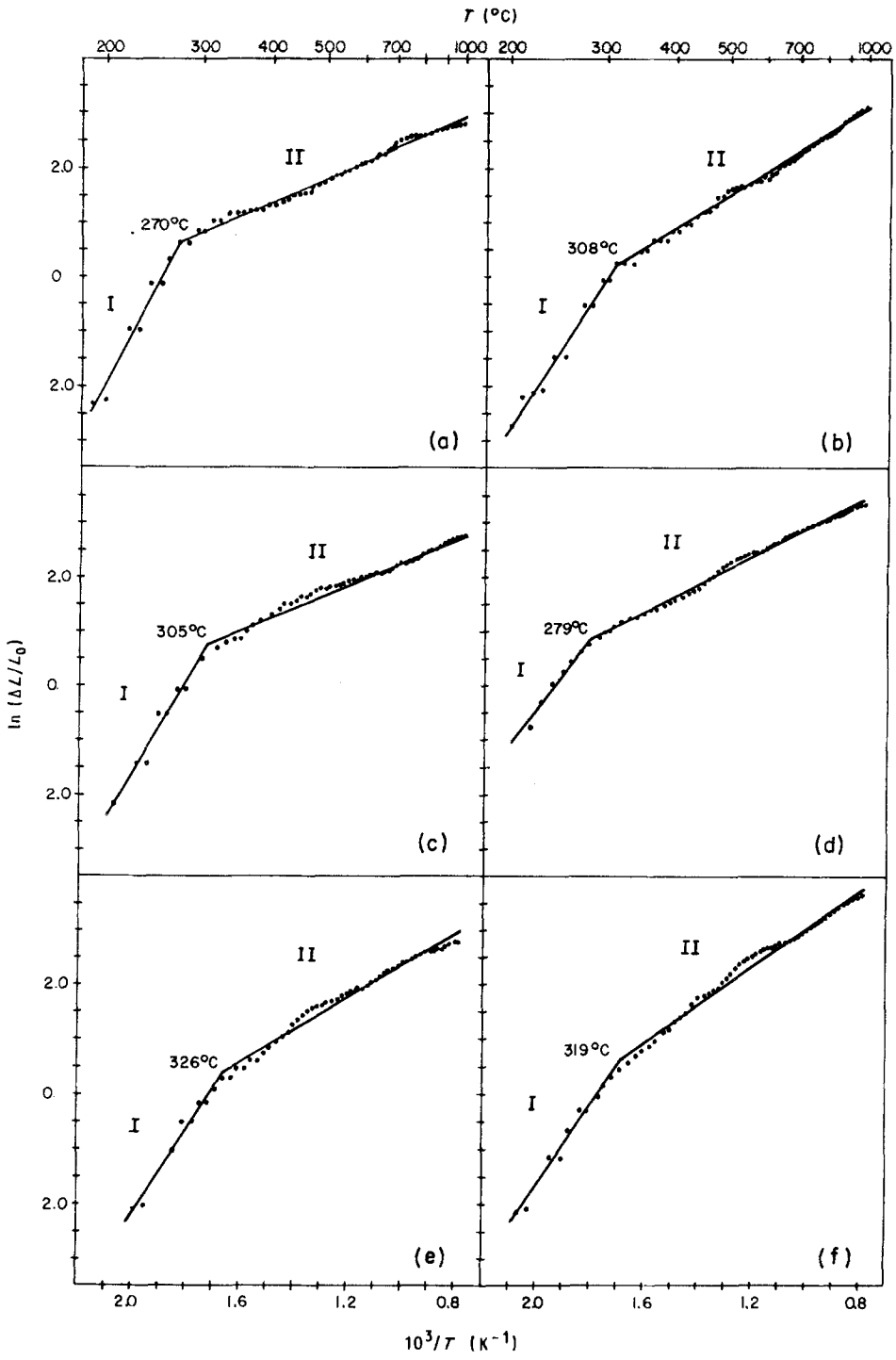

Figure 9 Logarithmic representation of linear contractions as a function of the inverse of absolute temperature for samples (a) 1.1, (b) 1.2, (c) 1.3, (d) 1.4, (e) 1.5, (f) 1.6.

samples in terms of relatively great initial weight loss correlated to a small linear contraction at low temperatures (up to 250–300° C). Later on, apart from a few fluctuations, a progressively increasing contraction is produced, with considerable weight losses.

Considering densification as an activated process and bearing in mind the constant rate of heating technique (CRH) [34], the representation of $\ln (\Delta L/L_0) = f(1000/T)$ indicates, by means of a series of straight lines, the different steps taking place in the overall densification process. Each step is characterized by a straight line with varying slopes depending on two factors, Q and n. Q denotes the apparent activation energy of the process and n is an exponent of the sintering law controlling the densification mechanism. Variation of the slope of the straight lines causes Q and/or n to vary triggering changes in the mechanism operative in each temperature range.

The overall activation energy involved in the densification process for each step is defined in the following equation

$$E_a = -1000mR \quad (1)$$

where m is the slope of the straight lines in the logarithmic representation of linear contraction plotted against the inverse of absolute temperature, and R is the gas constant.

In Fig. 9 $\ln (\Delta L/L_0)$ is shown as a function of the

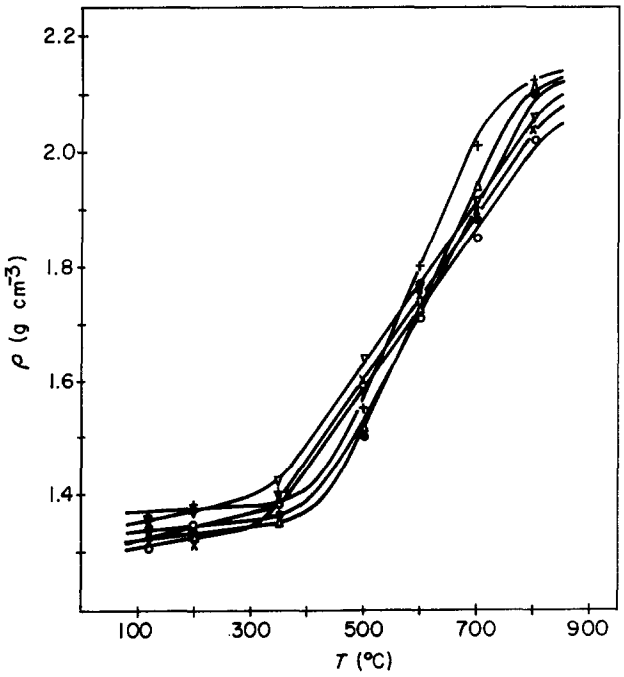

Figure 10 Thermal evolution of densities. (○ 1.1, ● 1.2, + 1.3, × 1.4, ▽ 1.5, △ 1.6).

inverse of the absolute temperature ($1000/T$) for each sample calculated from the linear contraction curves. The points obtained have been adjusted to straight lines which approximately represent the successive phases throughout the overall densification process.

TABLE IV Activation energy values calculated from the representations $\ln (\Delta L/L_0) = f(1000/T)$

Sample	E_a (kJ mol^{-1} K^{-1})	
	Segment I	Segment II
1.1	80.56	17.84
1.2	62.58	25.73
1.3	71.05	17.49
1.4	55.36	20.87
1.5	64.29	24.24
1.6	61.71	29.34

The activation energies calculated by means of Equation 1 are listed in Table IV.

In all samples two segments can be observed, which in turn, are indicative of the existence of two different mechanisms operating during densification. Up to temperatures between 279 and 326° C, segments I, losses of water and alcohols occur, which had been adsorbed to the material surface as well as release of the nitrate groups from the alkaline oxide precursors. The activation energies in the first densification stage are in the order of 55–80 kJ mol^{-1} K^{-1} and can be related to an elimination mechanism due to closure of the capillary system involving the groups that do not form part of the end material. Weight loss is likewise increased during this stage. The segments II, which range from the upper limit of segments I up to 990° C (the maximum reached in dilatometry), distinguish themselves by lesser activation energies as compared

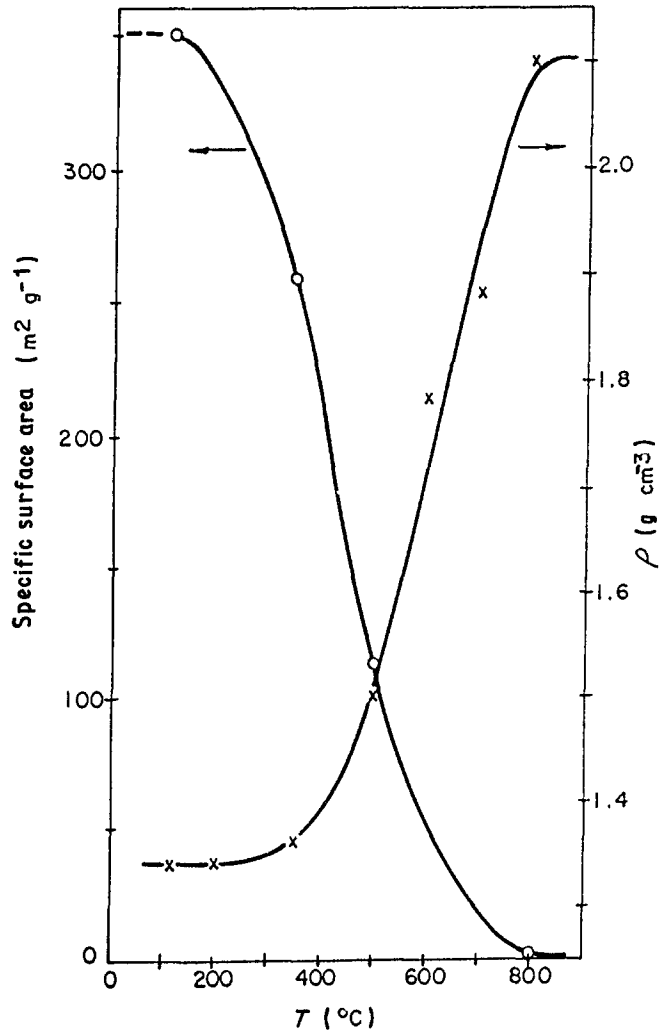

Figure 11 Thermal evolution of density and specific surface area for sample 1.2.

to those for segments I (17–29 kJ mol^{-1} K^{-1}). The weight losses in this second densification stage are generally less abrupt. The mechanism which is operative in this case may be a condensation–polymerization process of silanol groups to form Si–O–Si bonds. In all samples there are fluctuations in the general pattern around 500–600° C, probably due to the relaxation processes originated by the building up of the α-quartz and α-cristobalite networks [11]. In this case the fluctuations occur at lower temperatures than the crystallization in the DTA diagrams [11] as a consequence of the lower heating rate at which the dilatograms were recorded.

Samples 1.1 and 1.3 (with K_2O and Li_2O, respectively) show the greatest activation energies in their segments I, whereas in segments II they show the lowest activation energies of the series (Table IV). This would mean that, on the whole, the K_2O and Li_2O containing samples are characterized by a more progressive adsorbed water and alcohol loss, as they contain the type of alkaline ions which have a stronger water retention capacity (Li^+) or retain greater amounts in their environment (K^+) [14]. Thus the material is conditioned for better subsequent silanol groups condensation. As has been mentioned above, the Na_2O samples, however, are the ones that have to eliminate the larger amount of water. In this latter case the contractions produced are greater and more abrupt and account for a more irregular densification process requiring greater activation energies.

At temperatures above the experimental range a densification process of the viscous flow type is to be expected. In this R_2O–SiO_2 samples, 95 mol % are SiO_2, which delays sintering or shifts it to higher temperatures by viscous flow. As has been demonstrated elsewhere [35], in the B_2O_3–SiO_2 samples, however, a viscous flow type densification is possible at temperatures below 990° C thanks to the presence of B_2O_3 which favours the sintering process.

Fig. 10 shows the thermal evolution of sample density. Up to 350° C density practically does not vary, as nitrate groups are merely eliminated as well as adsorbed water and alcohols. As of this temperature, however, the silica skeleton begins to densify progressively, getting rid of structural water from the silanol groups. This is indicative that densification is principally achieved through a condensation–polymerization of the silanols starting at around 350° C. Fig. 11 shows the thermal evolution of the specific surface area of gel 1.2 together with the density variations of that sample. It can be observed that as of 350° C material densification sets in, since density values begin to increase remarkably and specific surface area diminishes until reaching values below 1 m^2 g^{-1} at 800° C. The evolution of the specific surface area of the other samples is similar to that of gel 1.2.

4. Conclusions

IR spectroscopy proved that the structure of vitreous materials of the R_2O–SiO_2 system corresponds to that of a silica network, as the alkaline ions practically are not incorporated, thus diverging from the classical scheme of conventional glasses obtained through melting. During the densification process and following the loss of adsorbed molecules and nitrate groups, a progressive condensation–polymerization occurs in the silanol groups up to 900° C and above. Thus a particulate silica material is constituted, which crystallizes mainly as α-cristobalite and eventually as α-quartz around 500° C. The alkaline ions may be retained in the interstitial gaps. Heat treatments in an inert atmosphere reduce residual structural water, especially if the treatment is carried out in a helium atmosphere. In this case, in addition, the silica crystallizations are eliminated.

References

1. J. PHALIPPOU, M. PRASSAS and J. ZARZYCKI, *J. Non-Cryst. Solids* **48** (1982) 17.
2. M. PRASSAS, J. PHALIPPOU, L. L. HENCH and J. ZARZYCKI, *ibid.* **48** (1982) 79.
3. M. PRASSAS, J. PHALIPPOU and L. L. HENCH, *ibid.* **63** (1984) 375.
4. G. F. NEILSON and M. C. WEINBERG, *ibid.* **63** (1984) 365.
5. M. PRASSAS and L. L. HENCH, in "Ultrastructure Processing of Ceramics, Glasses and Composites" (John Wiley, New York, 1984) p. 100.
6. Z. CONGSHAN, J. PHALIPPOU and J. ZARZYCKI, *J. Non-Cryst. Solids* **82** (1986) 321.
7. F. BRANDA, A. ARONNE, A. MAROTTA and A. BURI, *J. Mater. Sci. Lett.* **6** (1987) 203.
8. M. A. VILLEGAS and J. M. FERNANDEZ NAVARRO, *Bol. Soc. Esp. Ceram. Vidr.* **26** (1987) 99.
9. S. H. WANG and L. L. HENCH, *Mater. Res. Soc. Symp. Proc.* **32** (1984) 71.
10. L. L. HENCH, *ibid.* **32** (1984) 101.
11. M. A. VILLEGAS and J. M. FERNANDEZ NAVARRO, in Proceedings of the First International Workshop on Non-Crystalline Solids, San Feliú, May 1986, edited by M. D. Baró and N. Clavaguera (World Scientific Publishing, Philadelphia, 1986) p. 433.
12. D. RAVAINE, J. TRAORE, L. C. KLEIN and I. SCHWARTZ, *Mater. Res. Soc. Symp. Proc.* **32** (1984) 139.
13. D. RAVAINE, A. SEMINEL, Y. CHARBOUILLOT and M. VINCENS, *J. Non-Cryst. Solids* **82** (1986) 210.
14. M. A. VILLEGAS and J. M. FERNANDEZ NAVARRO, *Bol. Soc. Esp. Ceram. Vidr.* **26** (1987) 235.
15. M. C. WEINBERG and G. F. NEILSON, *J. Mater. Sci.* **13** (1978) 1206.
16. G. F. NEILSON, M. C. WEINBERG and G. L. SMITH, *J. Non-Cryst. Solids* **82** (1986) 137.
17. A. YASUMORI, S. INOUE and M. YAMANE, *ibid.* **82** (1986) 177.
18. L. L. HENCH, M. PRASSAS and J. PHALIPPOU, *ibid.* **53** (1982) 183.
19. K. SUSA, I. MATSUYAMA, S. SATOH and T. SUGANUMA, *ibid.* **79** (1986) 165.
20. E. M. RABINOVICH, D. L. WOOD, D. W. JOHNSON, Jr, D. A. FLEMING, S. M. VINCENT and J. B. MACCHESNEY, *ibid.* **82** (1986) 42.
21. D. M. KROL, C. A. M. MULDER and J. G. VAN LIEROP, *ibid.* **86** (1986) 241.
22. M. DECOTTIGNIES, J. PHALIPPOU and J. ZARZYCKI, *J. Mater. Sci.* **13** (1984) 2605.
23. M. A. VILLEGAS and J. M. FERNANDEZ NAVARRO, *ibid.* (accepted, in press).
24. D. M. HAALAND and C. J. BRINKER, *Mater. Res. Soc. Symp. Proc.* **32** (1984) 267.
25. R. JABRA, J. PHALIPPOU and J. ZARZYCKI, *Rev. Chim. Min.* **16** (1979) 245.
26. M. NOGAMI and Y. MORIYA, *J. Non Cryst. Solids* **48** (1982) 359.
27. H. H. W. MOENKE, in "The Infrared Spectra of Minerals" (Mineralogical Society, London, 1974) p. 365.
28. D. M. DODD and D. B. FRASER, *J. Appl. Phys.* **37**

(1966) 3911.
29. R. F. BARTHOLOMEW, B. L. BUTLER, H. L. HOOVER and C. K. WU, *J. Amer. Ceram. Soc.* **63** (1980) 481.
30. R. F. BARTHOLOMEW, *J. Non-Cryst. Solids* **56** (1983) 331.
31. J. ACOCELLA, M. TOMOZAWA and E. B. WATSON, *ibid.* **65** (1984) 355.
32. D. L. WOOD, E. M. RABINOVICH, D. W. JOHNSON, Jr, J. B. MACCHESNEY and E. M. VOGEL, *J. Amer. Ceram. Soc.* **66** (1983) 693.
33. F. ORGAZ and H. RAWSON, *J. Non-Cryst. Solids* **82** (1986) 57.
34. J. L. WOOLFREY and M. J. BANNISTER, *J. Amer. Ceram. Soc.* **55** (1972) 390.
35. M. A. VILLEGAS and J. M. FERNANDEZ NAVARRO, *J. Mater. Sci.* (accepted, in press).

Received 21 December 1987
and accepted 6 May 1988